Int J Adv Manuf Technol (2016) 87:2195–2211
DOI 10.1007/s00170-016-8542-3

ORIGINAL ARTICLE

An accelerated explicit method with GPU parallel computing for thermal stress and welding deformation of large structure models

Ninshu Ma [1,2]

Received: 15 December 2015 / Accepted: 19 February 2016 / Published online: 21 March 2016

Abstract To simulate welding induced transient thermal stress and deformation of large scale FE models, an accelerated explicit method (ACEXP) and graphical processing units (GPU) parallel computing program of the finite element method (FEM) were developed. In the accelerated explicit method, a two-stage computation scheme is employed. The first computation stage is based on a dynamic explicit method considering the characteristics of the welding mechanical process by controlling both the temperature increment and time scaling parameter. In the second computation stage, a static equilibrium computation scheme is implemented after dynamic thermal loading to obtain a static solution of transient thermal stress and welding deformation. It has been demonstrated that the developed GPU parallel computing program has a good scalability for large-scale models of more than 20 million degrees of freedom. The validity of the accelerated explicit method is verified by comparing the transient thermal stress and deformation with those computed by an implicit FEM. Finally, welding deformation and residual stress in a structure model assembled from nine high-strength steel plates and 26 weld lines were efficiently analyzed by ACEXP and GPU parallel computing within 45 h. The computed welding deformation agreed well with measured results, and a good accuracy was obtained.

Keywords Accelerated explicit method · GPU parallel computing · Thermal stress · Welding deformation · Large scale models · Welded structure

✉ Ninshu Ma
ma.ninshu@jwri.osaka-u.ac.jp; ma.ninshu@jsol.co.jp

[1] Osaka University, 11-1 Mihogaoka, Ibaraki, Osaka 567-0047, Japan

[2] JSOL Corporation, 2-2-4 Tosaori, Nishi-ku, Osaka 550-0001, Japan

1 Introduction

It is well known that welding residual stress and deformation have a significant influence on fatigue strength of welded joints [1]. Lai et al. [2] investigated the failure modes of fatigue cracking in welded structures. Dong and Hong [3] proposed the master S-N curve in the fatigue analysis for welded joints in large engineering structures. All these researches indicated that the computation for welding deformation and residual stresses in welded structures is essential for strength evaluation. Early pioneers in the computational welding mechanics Ueda et al. [4–6], Hibbit et al. [7], Goldak et al. [8], and Jonsson et al. [9] started their researches and applications of the finite element method in the 1970s–1980s. Since Ueda and Yamakawa [4] proposed a thermal elastic–plastic material model for welding thermal stress based on the static implicit finite element method, the implicit finite element method was mainly used for welding thermal-mechanics coupling simulations. Brown and Song [10] simulated the welding deformation and residual stresses of 1-m ring structure, which was a large model at that time. Lindgren et al. [11] reduced the computer time by applying dynamic meshing scheme to the implicit FEM. Nishikawa et al. [12] reduced computation time with a fast iterative substructure method (ISM) in which the global FE model was divided into a small model with large linear zones and a large model with small nonlinear zones according to the transient temperature distribution during welding. Lindgren [13] indicated that parallel computing used in implicit finite element methods can reduce the computer time and that used in explicit finite element methods had better scalability. Murakawa et al. [14], Deng et al. [15],

Wang et al. [16], and Ma et al. [17] computed welding distortion in large structures by both thermal elastic plastic FEM and efficient inherent strain method. Vega et al. [18] investigated the thermal deformation induced by line heating using inherent deformation parameters. Goldak and Asadi [19] presented some computation approaches to welding procedure optimization to minimize the welding deformation. They suggested that parallel computing is a key technology for both computational welding mechanics and optimization processing to reduce the computation time. Recently, Murakawa et al. [20] developed the inherent strain-based ISM named as i-ISM in which a temporary constraint on nodal displacements located in the zones away from the welding line was applied in the thermal elastic–plastic FE analysis. Since this temporary constraint has little effect on local plastic strains (inherent strain) near the welding zone, the final welding deformation and stresses without this constraint can be obtained by releasing it elastically. Huang et al. [21] modified the ISM and implemented large strain terms for the welding deformation computation in lap joints of thin plates. With the aid of the implicit FEM enhanced by ISM, Ma et al. [22, 23] analyzed residual stresses in butt joints due to laser arc hybrid welding and the effect of jig constraint on reduction of welding deformation. Furthermore, Ma et al. [24] considered martensite phase transformation in the analysis of flash butt welding induced residual stresses of high-carbon rail steels. Generally, the implicit FEM with an accurate material model for thermal elastic–plastic behaviors considering the phase transformation has a good accuracy in computing welding distortion and residual stress. On the other hand, the implicit FEM needs the large computer memory and its computing time for large-scale models is very long. Therefore, the implicit FEM is mainly employed to simulate the welding-induced thermal elastic–plastic behaviors in small-scale models.

Compared with the implicit FEM, Hallquist [25] developed a dynamic explicit FEM for computational impact mechanics. Since the explicit FEM needs a small amount of computer memory and its parallelized program has a good performance, it has been successfully used to simulate dynamic phenomena of very large automobile structures under impact loading. Mahin et al. [26] tried to simulate welding thermal stresses using the dynamic explicit method with a scaled mass and stress relaxation scheme. Although a small-scale two-dimensional FE model was selected, the computation time was not short. This is because the welding cooling time is too long to use the conventional dynamic explicit FEM with very small explicit time step. Ma et al. [27] employed a dynamic explicit FEM with a mass scaling technique and multi-CPU for the prediction of welding-induced buckling distortions in a butt joint of thin aluminum sheets. Ma and Umezu [28] summarized the techniques of using commercial dynamic explicit FEM software for the simulation of the welding thermal deformation. However, the commercial dynamic explicit FEM software cannot consider the welding characteristics such as the filling of the welding metals. Recently, Shibahara et al. [29] proposed an idealized explicit finite element method using an assumed mass matrix and a damping matrix for the simulation of the quasi-static welding thermal stress and deformation. Ikushima et al. [30] employed graphical processing units (GPU) for parallel computation and simulated welding residual stresses produced in a large-scale multi-pass butt-welded joint of thick plates. The existing approach of the explicit FEM to welding induced thermal elastic–plastic behaviors under fast heating and slow cooling process, used a very small explicit time step or an assumed large mass, the computing time and the accuracy for the large welding deformation of thin-walled structures become main issues which must be solved.

In the current work, an accelerated explicit method with a two-stage computation scheme was developed for simulating transient thermal stress as well as deformation occurring in welding heating and cooling processes. The first computation stage is based on the dynamic explicit FEM considering the characteristics of welding mechanical processes by controlling both the temperature increment and time scaling parameter. In the second computation stage, a static equilibrium computation scheme based on a dynamic relaxation algorithm was implemented after thermal loading in order to obtain a static solution of transient thermal stress and welding deformation. In this two-stage computation scheme, a damping parameter is automatically determined using the transient radial eigenvalue computed from nodal velocities of the finite element model. The scalability of developed GPU parallel computing program for large scale models of more than 20 million degrees of freedom was tested. The validity of the developed accelerated explicit method was verified by comparing the transient thermal stress and welding deformation with those obtained by an implicit FEM. Finally, the welding deformation and residual stress in a structure model assembled from nine high-strength steel plates and 26 weld lines were computed, and the results were compared with measured ones.

2 Accelerated explicit method with a two-stage computation scheme

2.1 General dynamic explicit FEM

A general equation of motions of particles in vector form according to Newton's laws of motion is given as follows:

$$Ma = F \tag{1}$$

In the Eq. (1), M, a, and F are a mass matrix, an acceleration vector, and a force vector of particles, respectively.

In the dynamic explicit method, the force vector includes the external force vector F_{ext} at current time $(t+dt)$, the internal residual force vector F_{int} at previous time (t), and the damping force F_{damp} in controlling dynamic vibration for quasi-static

problems. Therefore, the Eq. (1) can be extended to Eq. (2).

$$Ma(t+dt) = F_{ext}(t+dt) - F_{\text{int}}(t) - F_{damp}(t) \quad (2)$$

If the above motion equation is combined with FEM, the diagonal mass matrix M, the equivalent external nodal force $F_{ext}(t+dt)$, the equivalent internal nodal force $F_{\text{int}}(t)$, and the damping nodal force $F_{damp}(t)$ can be computed by following equations,

$$M = \int_{Vol} \rho\{N_i N_i\}^T \cdot dVol \quad (3)$$

$$F_{ext}(t+dt) = P_{\text{concentrate}}(t+dt) + P_{\text{pressure}}(t+dt) \quad (4)$$

$$F_{\text{int}}(t) = \int_{\text{Vol}} B \cdot \sigma(t) \cdot dVol \quad (5)$$

$$F_{\text{damp}}(t) = C \cdot v(t) \quad (6)$$

Where, ρ, N_i, Vol are the mass density of materials, the shape function of element and the volume of finite element model; the external nodal force $F_{ext}(t+dt)$ includes the concentrated nodal force $P_{\text{concentrate}}$, the nodal force due to external pressure P_{pressure}, and others such as the contacting nodal force; B is a matrix describing the relation between strains at integration points and nodal displacements in an element; σ is the stress vector in elements.

To solve the motion in Eq. (2), a very small time increment dt given by the following equation must be used according to the Courant-Frederic's-Lewy Condition [31].

$$dt \leq \frac{L_e}{c} \quad (7)$$

Where, the L_e in the above equation is the equivalent length of elements, and c is the propagation speed of stress wave in materials given by following equation.

$$c = \sqrt{\frac{E(1-\nu)}{(1+\nu)(1-2\nu)}\frac{1}{\rho}} \quad (8)$$

Where, E and v are the Young's modulus, and Poisson's ratio.

2.2 Accelerated explicit method with a two-stage computation scheme

It is well known that the time increment dt used in the explicit FEM, which is calculated by Eq. (7), is the order of 10^{-7} s for steels if the element size is about 1.0 mm. If the real loading time is the order of more than 1000 s, the computation cycles of explicit FEM can be the order of more than 10^{+10} and the computation may not ended within the acceptable time. Since the time of a welding thermal process can be the order of hours, the standard explicit FEM is quite difficult to adopt to simulate the thermal stress and welding deformation. To simulate mechanical phenomena occurring in welding thermal cycles, a two-stage computation scheme, using the explicit FEM on the accelerated explicit time domain and an equilibrium computation for static solution, was developed as schematically shown in Fig. 1. The accelerated explicit time domain Δt^{ACEXP} is determined with consideration of both the real time interval Δt^{real} and temperature increment in welding thermal cycles. This simulation method is here called the accelerated explicit method abbreviated to ACEXP for easy description in the following sections. If the 2nd stage equilibrium computation is skipped, the method becomes an explicit method for dynamic solution under the accelerated time domain. By the way, the thermal conduction analysis was performed before the stress analysis and is not discussed here.

2.2.1 Accelerated explicit time domain

To apply the explicit method to mechanical phenomena under the long time (e.g., 1000 s or more) thermal loading process shown in Fig. 2, the real time has to be scaled or accelerated many times without changing the thermal loads as schematically shown in Fig. 3. To distinguish the very small explicit time increment dt determined by Eq. (7), the real time increment denoted by Δt^{real}. The corresponding time interval in the accelerated explicit analysis is denoted by Δt^{ACEXP}. The symbols for real time and the time for the ACEXP method are denoted by t^{real}, t^{ACEXP}, respectively.

In this developed explicit method for stress and strain simulation, the accelerated explicit time interval Δt^{ACEXP} corresponding to the real time interval Δt^{real} is set by Eq. (9a) using the combination of the time-based scaling parameter t_{scale} and the temperature increment dT based time converting scheme with the consideration of the characteristics of welding thermal cycles.

$$\Delta t^{\text{ACEXP}} = \frac{\Delta t^{\text{real}}}{t_{\text{scale}}} + \frac{\Delta T_{\max}}{dT} dt \quad (9a)$$

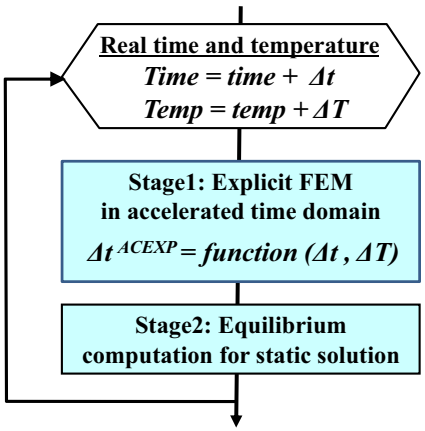

Fig. 1 A two-stage computation scheme of accelerated explicit method

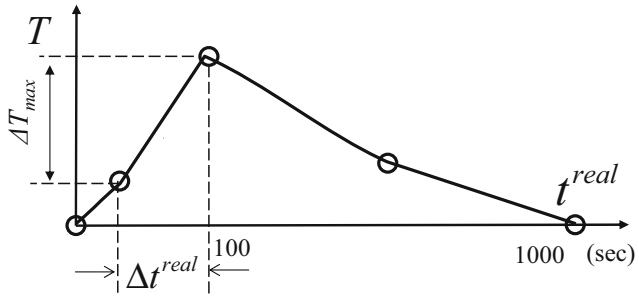

Fig. 2 An example of welding thermal cycle in the real time domain

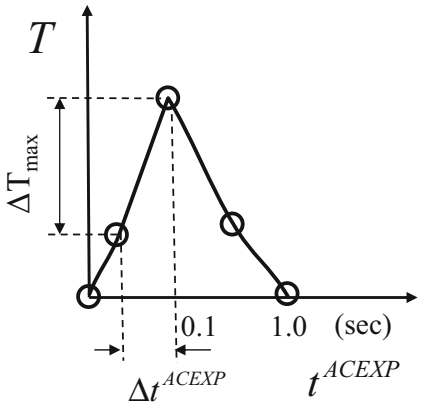

Fig. 3 An example of thermal cycle in the accelerated explicit time domain

Where, $\Delta T_{\max}$ is the maximum temperature change in the real time interval Δt^{real} and dt is the explicit time given by Eq. (7).

The first term in the Eq. (9a) uses the conventional mass scaling technique summarized by Ma and Umezu [28]. The second term is based on the temperature increment control method used in the implicit FEM [20]. Based on this time accelerating scheme, the explicit computation cycles or the computation time at the first stage will be controlled by the two parameters t_{scale} and dT. Their combination is better to control both the computation accuracy and computation time which is proportional to the explicit cycles. The parameters t_{scale} and dT can be approximately set to about 1000.0 and 0.1~1.0, respectively.

If the accelerated explicit time interval Δt^{ACEXP} was set, the total computing cycles T_{cycles} of the explicit method can be determined by Eq. (9b).

$$Tcycles = \Delta t^{\text{ACEXP}} \Big/ dt = \frac{1}{t_{\text{scale}}} \frac{\Delta t^{\text{real}}}{dt} + \frac{\Delta T_{\max}}{dT} \tag{9b}$$

2.2.2 Equilibrium computation scheme for static solution

Usually, the dynamic explicit solution does not satisfy the static mechanical equilibrium condition. Therefore, to obtain the static solution of welding thermal stress and deformation, an equilibrium computation is necessary. The implicit iteration scheme or a dynamic relaxation algorithm with repeating explicit cycles can be employed. Here, the dynamic relaxation algorithm based on the explicit computing method is selected. To save the computation time without losing the accuracy, the equilibrium computation can selectively conduct once every certain step intervals Nc as shown in Fig. 4.

During the equilibrium computation, the ratio E_{ratio} of kinematic energy to internal energy and the ratio U_{ratio} of the normalized displacement increment to the normalized total displacement of the FE model are defined by Eqs. (10)–(11), respectively. If the ratios E_{ratio} and U_{ratio} are less than their tolerances E_{tol} and U_{tol}, respectively, the results computed by ACEXP can be considered as a static solution.

$$E_{\text{ratio}} = \frac{\sum_{i=1}^{\text{Nodes}} \frac{1}{2} m v^2}{\sum_{ie=1}^{NE} \overline{\sigma} \cdot \overline{\varepsilon} \cdot V_e} < E_{\text{tol}} \tag{10}$$

$$U_{\text{ratio}} = \frac{\sum_{i=1}^{\text{Nodes}} \sqrt{\Delta u_x^2 + \Delta u_y^2 + \Delta u_z^2}}{\sum_{i=1}^{\text{Nodes}} \sqrt{u_x^2 + u_y^2 + u_z^2}} < U_{\text{tol}} \tag{11}$$

The tolerances E_{tol} and U_{tol} are the order of 10^{-4} for the accurate equilibrium computation.

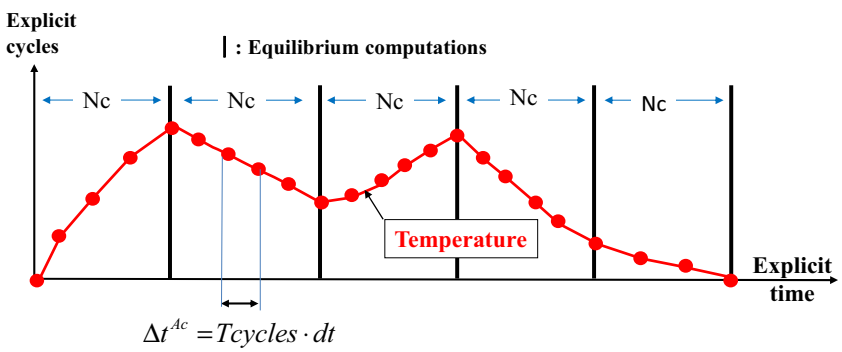

Fig. 4 Selective equilibrium computation scheme at the certain thermal step intervals Nc

2.2.3 Estimation of transient radial eigenvalue for damping parameter

It was reported by Ma and Umezu [28] that the effect of dynamic vibrations on the welding deformation can be well controlled by applying a mass damping force given by following equation based on the minimum radial eigenvalue $\omega_{\min}$.

$$F_{damp}(t) = 2.0\omega_{\min}\cdot M\cdot v(t) \tag{12}$$

To get the minimum radial eigenvalue $\omega_{\min}$ of a global FE model, generally, the eigenvalue analysis based on the implicit FEM has to be performed previously. If the degrees of freedom of FE models become too large, the memory requirement and computation time will be very long. On the other hand, the minimum eigenvalue computed by the implicit FEM may not fit the transient welding deformation mode which is changing during welding and subsequent cooling processes. For these reasons, an explicit estimation method for the dynamic eigenvalue was suggested by Papadrakakis [32]. By referring to this method, a transient radial eigenvalue $\omega_{\mathrm{def}}(t)$ corresponding to the transient welding deformation mode at time *(t)* is computed by Eq. (13). The parameter *g(t)* in Eq. (13) is computed using the integrated velocity from all nodes of a global FE model defined by Eqs. (14)–(15).

$$\omega_{def}(t) = \frac{|1-g(t)|}{dt\cdot\sqrt{g(t)}} \tag{13}$$

$$g(t) = \frac{v_g(t)}{v_g(t-dt)} = \frac{\sqrt{v_g^x(t)^2 + v_g^y(t)^2 + v_g^z(t)^2}}{\sqrt{v_g^x(t-dt)^2 + v_g^y(t-dt)^2 + v_g^z(t-dt)^2}} \tag{14}$$

$$v_g^x(t) = \frac{\sum_{i=1}^{\mathrm{Nodes}} M_i v_i^x(t)}{\sum_{i=1}^{\mathrm{Nodes}} M_i}, v_g^y(t) = \frac{\sum_{i=1}^{\mathrm{Nodes}} M_i v_i^y(t)}{\sum_{i=1}^{\mathrm{Nodes}} M_i}, v_g^z(t) = \frac{\sum_{i=1}^{\mathrm{Nodes}} M_i v_i^z(t)}{\sum_{i=1}^{\mathrm{Nodes}} M_i} \tag{15}$$

Where, $v_g(t)$ and $v_g(t-dt)$ are the integrated velocities at time (t) and at time $(t+dt)$, respectively.

Using the transient radial eigenvalue $\omega_{def}(t)$, the damping force in the developed accelerated explicit method is given by the following equation.

$$F_{damp}(t) = 2.0\omega_{def}(t)\cdot M\cdot v(t) \tag{16}$$

2.3 Stress and strain computation

When the acceleration $a(t+dt)$ at the nodes of FEM using Eq. (2) is obtained, the nodal velocity $v(t+dt)$, the nodal displacement increment $du(t+dt)$ can be easily computed in sequence by Eq. (17) and Eq. (18), respectively.

$$v(t+dt) = v(t) + a(t+dt)\cdot dt \tag{17}$$

$$du(t+dt) = v(t+dt)\cdot dt \tag{18}$$

Then, the strain increment $d\varepsilon(t+dt)$ at the integration points of elements can be computed by following equation.

$$d\varepsilon(t+dt) = B\cdot du(t+dt) \tag{19}$$

Where, B is the matrix describing the relationship between strain and nodal displacement in an element.

The thermal stress $\sigma(t+dt)$ can be computed based on thermal elastic plastic theory using the following equation:

$$\sigma(t+dt) = \sigma(t) + D(T)\cdot\left(d\varepsilon - d\varepsilon^T - d\varepsilon^p\right) \tag{20}$$

Where, the $d\varepsilon^T, d\varepsilon^p$ and $D(T)$ are the thermal strain increment, plastic strain increment, and material elastic matrix, respectively. The thermal strain increment and plastic strain increment are given by Eq. (21) and Eq. (22), respectively.

$$d\varepsilon^T = \alpha(T)\cdot dT + \frac{dD(T)}{dT}D^{-1}(T)\cdot\sigma(t)\cdot dT \tag{21}$$

$$d\bar{\varepsilon}^p = \frac{\bar{\sigma}_{try}(t+dt) - \sigma_Y\left(T+dT, \bar{\varepsilon}^p\right)}{3G(T)+H'(T)}, \; d\varepsilon_{ij}^p = d\bar{\varepsilon}^p\frac{\partial\bar{\sigma}}{\partial\sigma_{ij}} \tag{22}$$

Where, $\alpha(T)$, $G(T)$ and $H'(T)$ are the transient thermal expansion coefficient, shear modulus, and plastic work hardening tangent coefficient of materials at the temperature (T). σ_Y is the yield stress of materials changing with the temperature and equivalent plastic strain. $\bar{\sigma}_{try}(t+dt)$ is the elastically trial equivalent stress when a radial return algorithm is employed for the stress update.

2.4 Flow chart of accelerated explicit FEM program

Based on the proposed accelerated explicit method, a FEM program was developed. The flow chart of accelerated explicit FEM program is shown in Fig. 5. The left side of the flow chart shows the main loop in which a temperature file for welding thermal cycles is read, the accelerating time interval $\Delta t^{\mathrm{ACEXP}}$ is determined and results are written out. The right side of the flow chart expresses the computation procedures from nodal acceleration to stress update of the accelerated

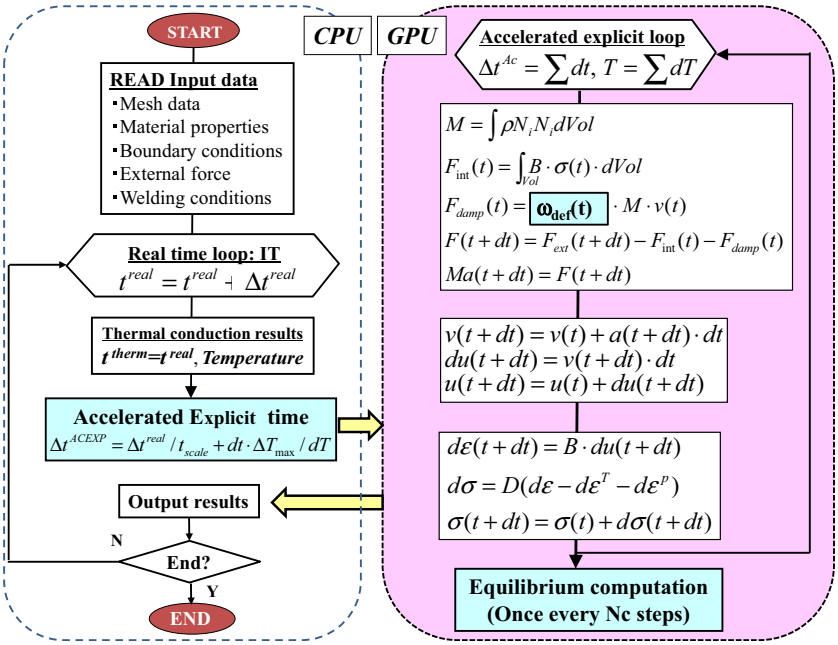

Fig. 5 Flow chart of accelerated explicit FEM program and its GPU parallel computing

explicit FEM. Since the work in the right side is just simple calculations, the parallel computing using multi-cores of CPU or GPU will greatly reduce the computation time.

When the thermal cycles for all nodes were read from a saved temperature file computed by thermal conduction FEM and the accelerated explicit time interval Δt^{ACEXP} was set, the acceleration $a(t+dt)$ can be easily computed using Eq. (2) with a very small explicit time step dt. Then, the velocity, displacement increment, strain increment, and stress are computed in sequence. When the accumulated explicit time $\sum dt$ reached the accelerated time interval Δt^{ACEXP}, the stabilization computation started. The new scheme used in this accelerated explicit method is emphasized in the flow chart by a light blue background. The computations are continued until the real time reached the end time defined in the input data.

Since this article is only focused on the analyzing method for transient thermal stress and welding deformation, the descriptions of implicit FEM for welding thermal conduction analysis are neglected. The nodal temperature and its change with time during welding and cooling processes are saved into a temperature file for stress and strain calculation using the ACEXP method.

2.5 GPU parallel computing FEM program

Generally, a personal computer (PC) has 4–8 CPU cores and a GPU board has more than 1000 cores (2496 cores for GPU Tesla-k20) for computation. Therefore, the computation performance should be greatly improved if the GPU parallel computing FEM program is developed. However, the memory of a GPU board is limited within 5GB-12GB which is much smaller than main PC's physical memory. Therefore, how to save memory usage is an important issue in programming for GPU parallel computing. The developed parallel computing FEM program using both CPU and GPU was shown in Fig. 5. The

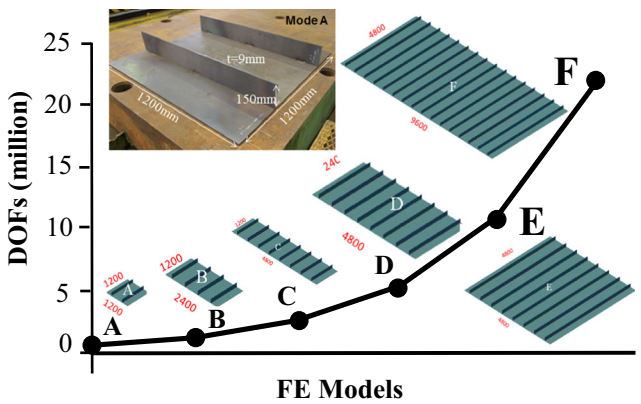

Fig. 6 Larger scale FE models of fillet welded structures

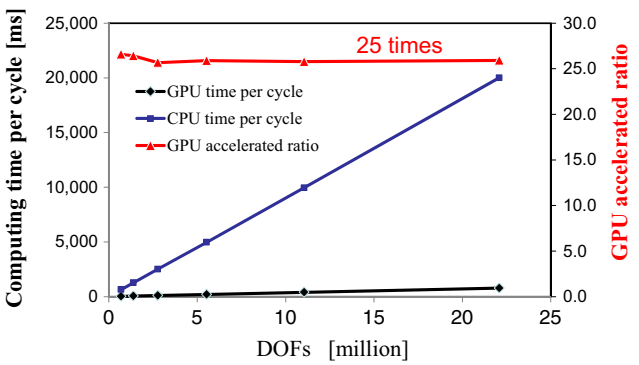

Fig. 7 Relation of DOFs and computation time using one board GPU and one core CPU

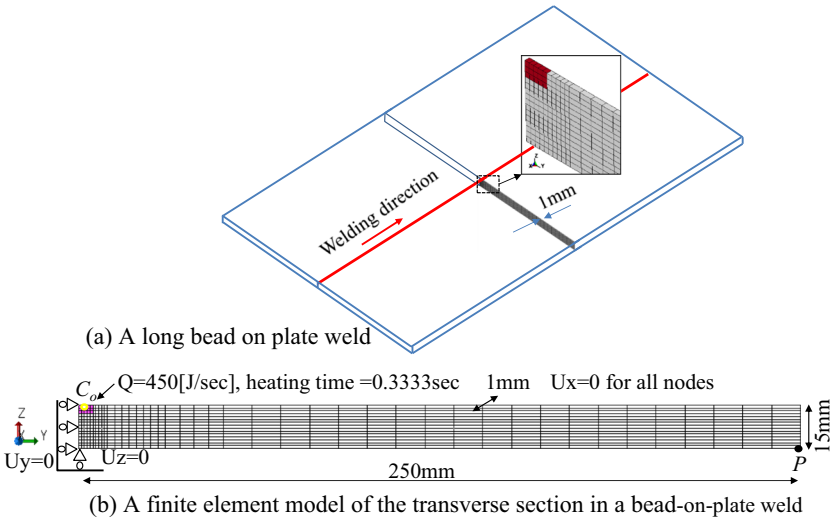

Fig. 8 A basic model of a long bead-on-plate weld

tasks in the left part of Fig. 5 are assigned to CPU, and those in the right part are assigned to GPU, respectively. Firstly, the heat conduction calculation with a large time step was performed in advance and the output data with temperature history was saved as a temperature file. Then, the temperature file becomes an input file for the subsequent stress analysis. CPU reads and writes data in time controlling loop and GPU conducts thermo-elastic–plastic calculation of nodal forces, nodal displacements, strains, and stresses in elements.

Using the FE models of fillet welds with DOFs changing from 0.7 million to 22 million represented in Fig. 6, the relation between DOFs of FE models and computation time of each accelerate explicit cycle was investigated as shown in Fig. 7. The marks ● and ■ in Fig. 7 show the computation time per explicit cycle using one GPU (tesla-k20) and one core CPU (Core i7), respectively. From the results of the all testing models, GPU computation time per cycle is about 1/25 of CPU. In the other word, the parallel computing efficiency using one GPU is 25 times compared with one CPU. This accelerated ratio is quite good.

3 Verification of ACEXP method using a basic model

3.1 Descriptions of a basic bead welding model

To verify the accuracy of the proposed accelerated explicit method, a section model of a very long bead welding plate of the mild steel is selected from a book [6] as shown in Fig. 8a. The model dimensions in the x, y, and z directions are 1, 250, and 15 mm, respectively. Considering the symmetry of the thermal stress and deformation in the width direction (y) of the weld line, a half model was employed. The mesh division and displacement boundary conditions are shown in Fig. 8b. Only one solid element in the welding direction (x) is divided and the x-displacement Ux at all nodes is constrained to describe the plane strain state of the model. In the thermal conduction simulation, an implicit FEM code JWRIAN enhanced by an iterative substructure method [20] was employed and a volume heat source with a uniform distribution in the rectangle prism (5.0 × 3.0 × 1.0 mm) was assumed. The total volume heat generation rate is 450 (J/s), and the heating time is 0.3333 s. The material physical

Table 1 Material physical-mechanical properties of the mild steel and their change with temperature

Temperature [°C]	0.0	200.0	400.0	600.0	800.0	1000.0	1200.0
Mass density [t/mm^3]	7.82E-9	7.79E-9	7.72E-9	7.66E-9	7.61E-9	7.61E-9	7.61E-9
Specific heat [J/t/°C]	408E + 3	533E + 3	658E + 3	783E + 3	908E + 3	908E + 3	908E + 3
Conductivity [J/mm/s/°C]	0.05317	0.0515	0.0465	0.0382	0.0265	0.0625	0.0625
Heat transfer coef [J/mm^2/s/°C]	1.0E-5	2.0E-5	4.0E-5	8.0E-5	15.0E-5	25.0E-5	25.0E-5
Thermal expansion α [1/°C]	1.0E-5	1.0E-5	1.0E-5	1.0E-5	1.0E-5	1.0E-5	1.0E-5
Young's modulus E [MPa)	2.0E + 5	2.0E + 5	2.0E + 5	2.0E + 5	2.0E + 4	2.0E + 4	2.0E + 3
Poisson's ratio υ	0.3	0.3	0.3	0.3	0.3	0.3	0.3
Yield stress SY [MPa]	200.0	200.0	200.0	200.0	2.0	2.0	2.0
Plastic hardening Etan [MPa]	2.0E + 3	2.0E + 3	2.0E + 3	2.0E + 3	2.0E + 2	2.0E + 2	2.0E + 2

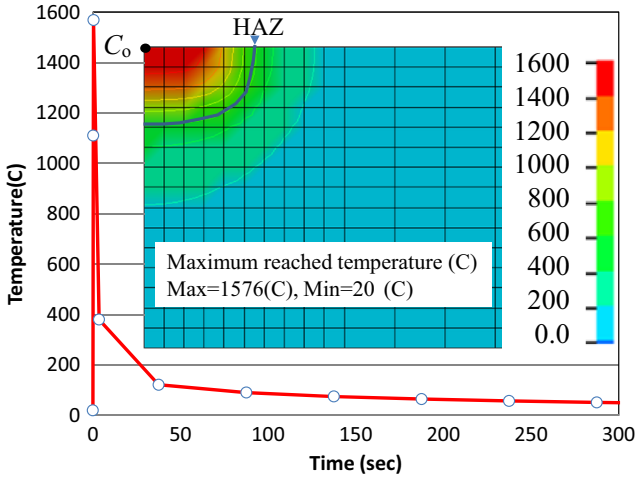

Fig. 9 Welding thermal cycle at point C_o and maximum temperature distribution in cross section

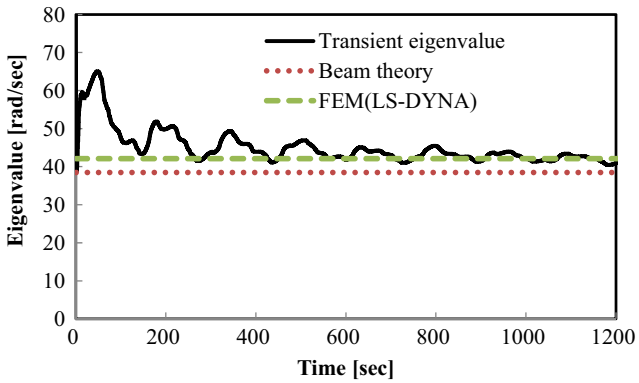

Fig. 10 Estimated transient radial eigenvalue and its change with time

properties (mass density, specific heat, thermal conductivity, heat transfer coefficient, linear thermal expansion coefficient), mechanical properties (Young's modulus, Poisson's ratio, Yield stress and linear hardening coefficient of plasticity) of the mild steel, and their change with temperature are shown in Table 1 [6]. The Young's modulus, yield stress, and linear hardening coefficient of plasticity of the mild steel at the room temperature are 2.0E + 05 MPa, 200 MPa, and 200 MPa, respectively. With increasing temperature, Young's modulus and Yield stress decrease. When the temperature is higher than about 800 °C which is so called the mechanical melting temperature, the Yield stress is assumed to be 1 % of the value at the room temperature.

3.2 Welding thermal cycles and temperature distribution

Figure 9 shows the thermal cycle at the point C_o in the welding zone computed by an implicit FEM code JWRIAN [20] for thermal conduction. The maximum reached temperature in the thermal cycle at the point C_o is 1576 °C which is slightly higher than the melting point of steel (1500 °C). Since the material in the thermal conduction analysis was assumed to be at the solid state and metal flow was not considered, the peak temperature is slightly higher than the melting point of the mild steel (1500 °C). The slightly higher temperature than the melting point has little influence on the welding distortion and residual stress [6]. The distribution contour of the maximum reached temperature around the welding zone is also shown in the same figure. The heat affected zone (>723 °C) marked by a solid line can be easily observed.

Fig. 11 Welding deformation mode during welding and cooling by ACEXP method

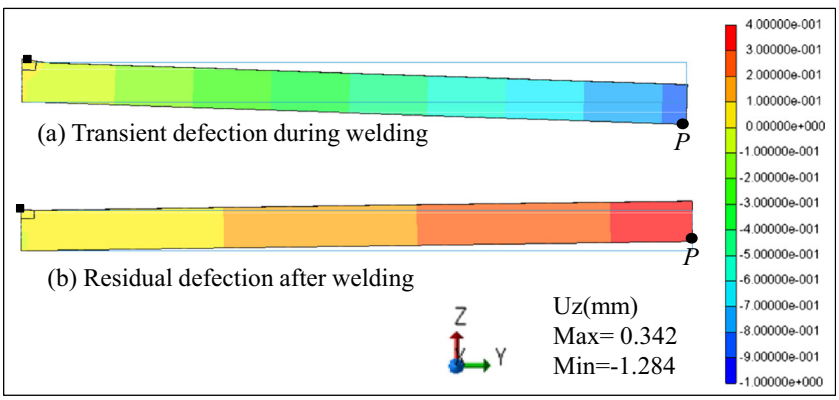

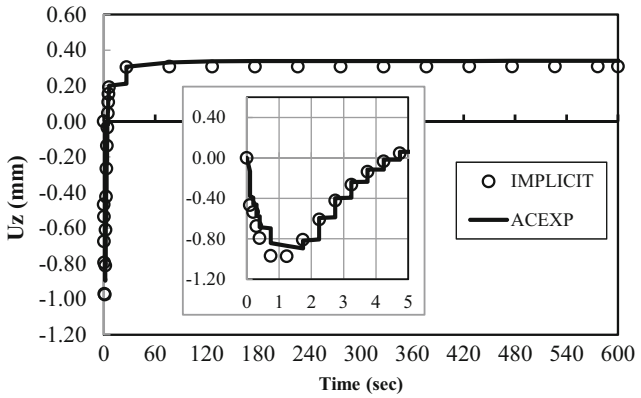

Fig. 12 History of z-displacement at edge point P during welding and subsequently cooling

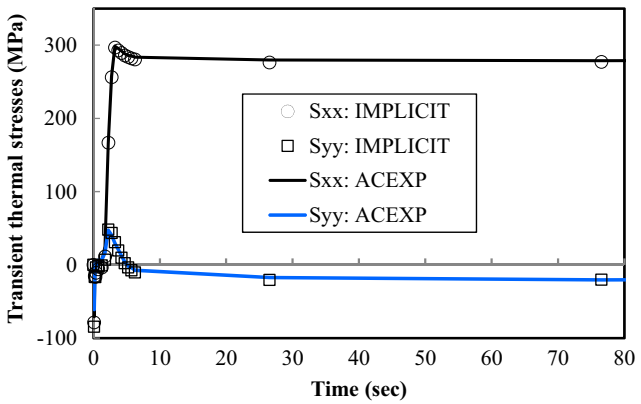

Fig. 13 History of thermal stress at welded zone during heating and cooling

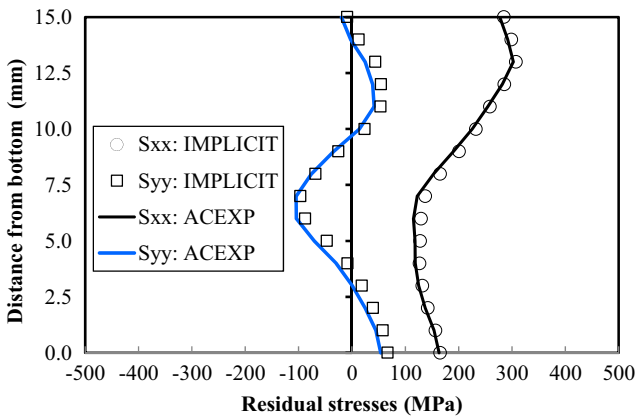

Fig. 14 Distributions of residual stresses through thickness direction

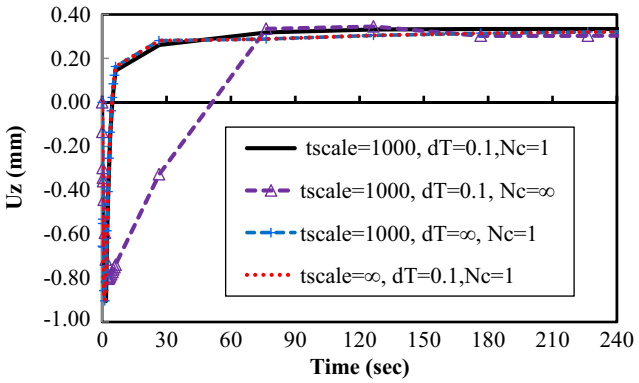

Fig. 15 Effect of controlling parameters on welding deformation

3.3 Transient radial eigenvalue

This basic bead welding model is close to a simple cantilever beam. The eigenvalue of the bending deformation mode in the z direction can be easily calculated using the Eq. (23) based the classical elastic vibration theory if the material properties (mass density scaled 1000 times, Young's modulus, and Poisson's ratio) at the room temperature shown in Table 1 are used.

$$\omega_{\mathrm{def}} = \frac{\lambda_1^2}{L^2}\sqrt{\frac{EI}{\rho \cdot \mathrm{Area}}} = \frac{1.875^2}{250^2}\sqrt{\frac{(2.0\times10^5)\times\left(15^3\cdot1\middle/12\right)}{1000\times(7.8\times10^{-9})\times(15\times1)}} \approx 39\left[\mathrm{rad}\middle/\mathrm{sec}\right] \tag{23}$$

The estimated transient radial eigenvalue $\omega_{\mathrm{def}}(t)$ by Eqs. (13)–(15) and its change with time are shown in Fig. 10. When the time is less than about 100 s, the transient

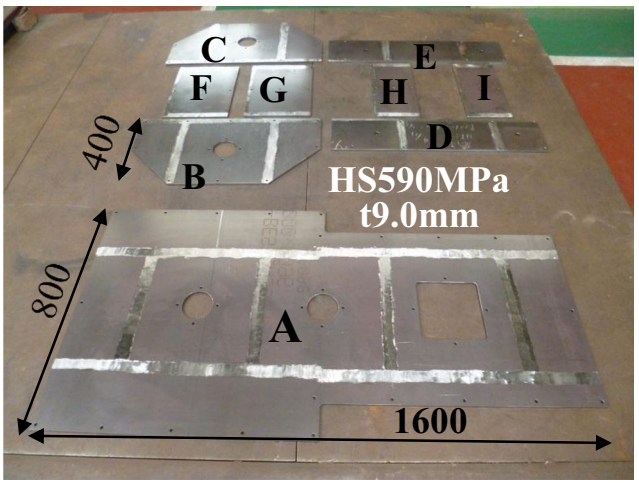

Fig. 16 Steel plates for welding structure assembly

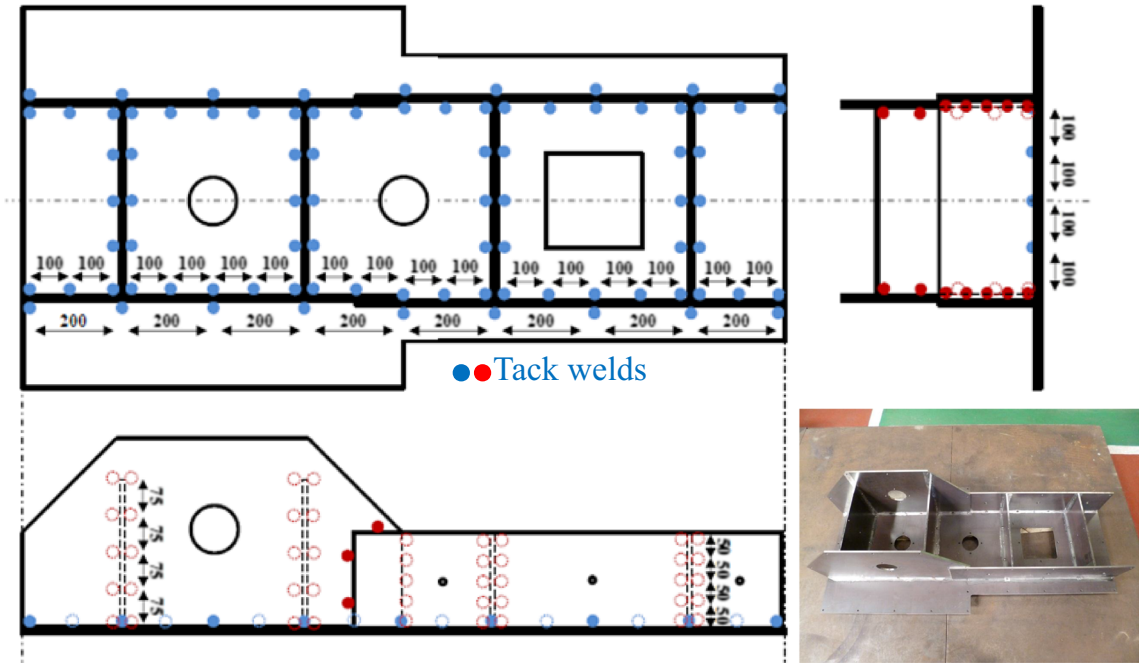

Fig. 17 The tack welded structure before regular welding

eigenvalue is larger. When the time is longer than about 100 s, the transient radial eigenvalue saturates to a constant value. For the comparison, the constant eigenvalue computed by Eq. (23) and that computed by eigenvalue analysis using commercial FEM software LS-DYNA are also represented in the same figure. A good agreement among the computed radial eigenvalues by three methods was obtained when the temperature becomes low in the cooling process.

3.4 Welding deformation and thermal stresses

To verify the proposed ACEXP method, the welding induced thermal stress and deformation were computed and compared with the results by the implicit FEM. In the ACEXP computation, the time scaling factor t_{scale} and temperature increment dT used in Eqs. (9a) and (9b) are set to be about 1000.0 and 0.1, respectively.

The transient deformation modes and the distribution of the z-displacement Uz (mm) during welding and after cooling, computed by the ACEXP method, are shown in Fig. 11. The z-displacement Uz(t) at the right edge point P of the model and its historical change with time are shown in Fig. 12. The welding deformation marked by cycles in Fig. 12 is the results computed by the implicit FEM. It can be easily observed that the results by the ACEXP method agreed very well with the implicit FEM. The vertical changes in the displacement-time curve shown in Fig. 12 represent the displacement due to the equilibrium computation for static solutions.

Figure 13 shows the historical changes of the transient thermal stresses Sxx and Syy in an element of the welded zone during heating and cooling process. The thermal stresses computed by ACEXP method agreed very well with the results by the implicit FEM. Figure 14 represents the distributions of

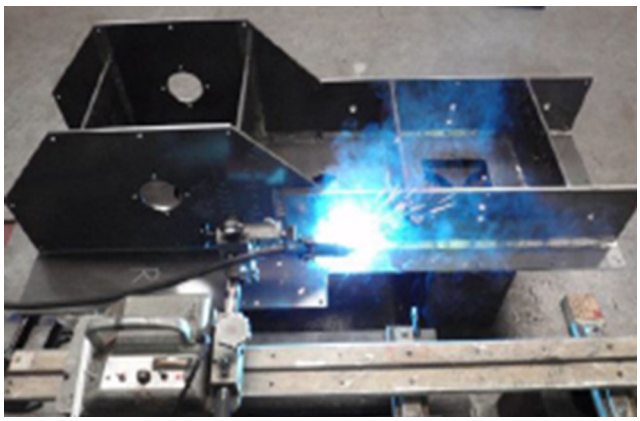

Fig. 18 Welding of the steel structure of construction machinery

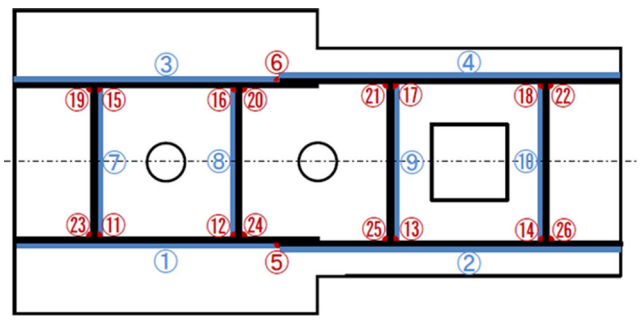

Fig. 19 Welding line numbers ①~□ and welding sequence

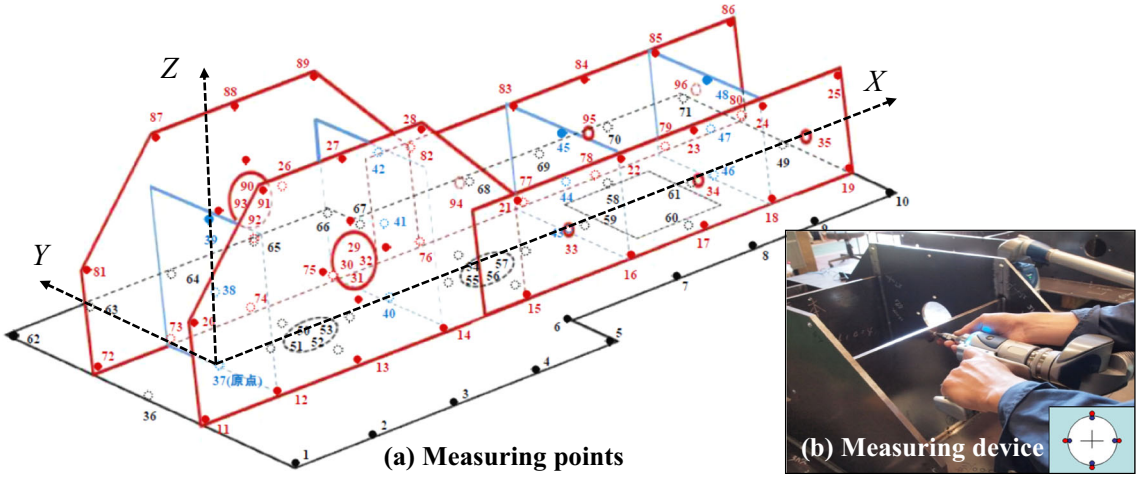

Fig. 20 Measuring points and method for welding deformation in the experiment

stresses Sxx and Syy through the thickness direction. The residual stresses computed by both the ACEXP method and implicit FEM are close each other.

3.5 Effect of controlling parameters

The transient computation of the ACEXP method is controlled by three parameters which are a time scaling parameter t_{scale}, temperature increment dT defined by Eqs. (9a) and (9b), and the equilibrium computation interval Nc. The referencing values of these parameters from the view of high accuracy are $t_{scale}=1000, dT=0.1, Nc=1$. Three additional computations were performed by changing these three parameters one by one. Figure 15 shows the transient displacement Uz(t) at the edge point P and the effect of these parameters. It can be observed that accelerating time control parameters t_{scale}, dT gave a limited influence on the transient deformation. When $Nc=\infty$, the equilibrium computation was performed only at the final step of thermal loading in order to keep the accuracy on residual results. From the Fig. 15, we observed that the interval parameter Nc for the equilibrium computation had a large effect on the transient deformation which saturated to a certain value slower than other computation cases. All parameters had a little influence on the residual deformation. This means that the computed residual deformation by the proposed ACEXP method is not sensitive to input parameters.

4 Welding deformation and residual stresses in a large structure model

4.1 The welded structure and deformation measuring method

Figures 16, 17, 18, and 19 show high strength (HS590) steel plates, the tack welded structure before regular welding, and the structure during welding and its welding sequence, respectively. The welding structure was assembled from nine steel plates with 9.0 mm in the thickness, whose tensile strength, yield strength, and elongation are 670 MPa, 537 MPa, and 28 %, respectively. The length, width and height of the welding structure are 1600, 800, and 400 mm, respectively. There are 26 weld lines and all weld lines were tacked first. The regular welding for weld lines ①~④ was performed by

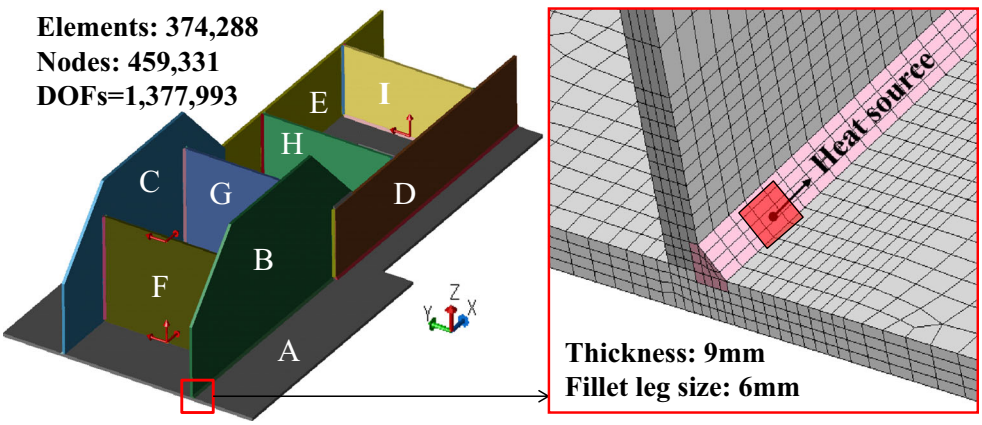

Fig. 21 FE model and its element division of the welded structure

Table 2 Material physical-mechanical properties of HS590 steel and their change with temperature.

Temperature [°C]	0.0	200.0	400.0	600.0	800.0	1000.0	1200.0
Mass density [t/mm^3]	7.82E-9	7.79E-9	7.72E-9	7.66E-9	7.61E-9	7.61E-9	7.61E-9
Specific heat [J/t/°C]	408E + 3	533E + 3	658E + 3	783E + 3	908E + 3	908E + 3	908E + 3
Conductivity [J/mm/s/°C]	0.05317	0.0515	0.0465	0.0382	0.0265	0.0625	0.0625
Heat transfer coef [J/mm^2/s/°C]	1.0E-5	2.0E-5	4.0E-5	8.0E-5	15.0E-5	25.0E-5	25.0E-5
Thermal expansion α [1/°C]	1.20E-5	1.25E-5	1.50E-5	1.35E-5	1.40E-5	1.45E-5	1.50E-5
Young's modulus E [MPa)	2.0E + 5	2.0E + 5	1.5E + 5	0.9E + 5	0.5E + 5	0.3E + 5	0.2E + 5
Poisson's ratio υ	0.3	0.3	0.3	0.3	0.3	0.3	0.3
Yield stress SY [MPa]	537.0	480.0	330.0	210.0	85.0	50.0	30.0
Plastic hardening Etan [MPa]	2.0E + 3	2.0E + 3	2.0E + 3	2.0E + 3	2.0E + 2	2.0E + 2	2.0E + 2

automatic arc welding process and that for weld lines ⑤~□ was done by manual arc welding. The shield gas in arc welding process was the metal active gas (MAG). The arc welding current, voltage, and welding speed are about 190A, 220 V, and 5 mm/s within ±10 % variation. The diameter of welding wire is ϕ1.2 mm, and its tensile strength, yield strength, and elongation are 690 MPa, 560 MPa, and 30 %, respectively.

To evaluate the practical welding deformation, the three dimensional coordinates at the 96 evaluating points as shown in Fig. 20a were measured two times after tack welding and regular welding, respectively. A contact type of the three dimensional coordinate measuring device FARO as shown in Fig. 20b was employed. The measuring accuracy is about ±0.03 mm. The coordinate changes at measuring points before and after regular welding are three displacement components Ux, Uy, and Uz for descriptions of welding deformation.

4.2 FE model of the welded structure

Figure 21 shows the mesh division and boundary conditions of FE model. Only six nodal displacement components drawn by arrows at three nodes are constrained in order to prevent the rigid movement of the specimen. A type of eight node solid element was used. The total number of elements, nodes, and degrees of freedom is, respectively, 374,288, 459,33,1 and 1, 377,993. The designed fillet leg size is 6 mm, and the minimum mesh size is 2 mm. A moving volume heat source was employed in the simulation for welding thermal conduction. The heat source has a uniform distribution in the moving volume highlighted by red color as shown in Fig. 21. The heat efficiency for all weld lines is assumed to be 60 % in the thermal conduction analysis. The steel plates were marked by A~I for easy descriptions.

4.3 Material properties and their change with temperature

To compute the welding deformation and residual stresses in the structure model assembled from high strength steel plates (HS590), material physical properties (mass density, specific heat, thermal conductivity, heat transfer coefficient including both convection and radiation, thermal expansion coefficient) in the previous thermal conduction analysis, and the mechanical properties (Young's modulus *E*, Poisson's ratio υ, Yield stress *SY* and linear plastic strain hardening coefficient *Etan*) were newly measured. The measured material properties and their change with temperature used in the simulation are shown in Table 2. The materials properties of weld metal (WM) were assumed to be the same as base metal (BM). At the high temperature over 1200 °C, the materials properties were considered

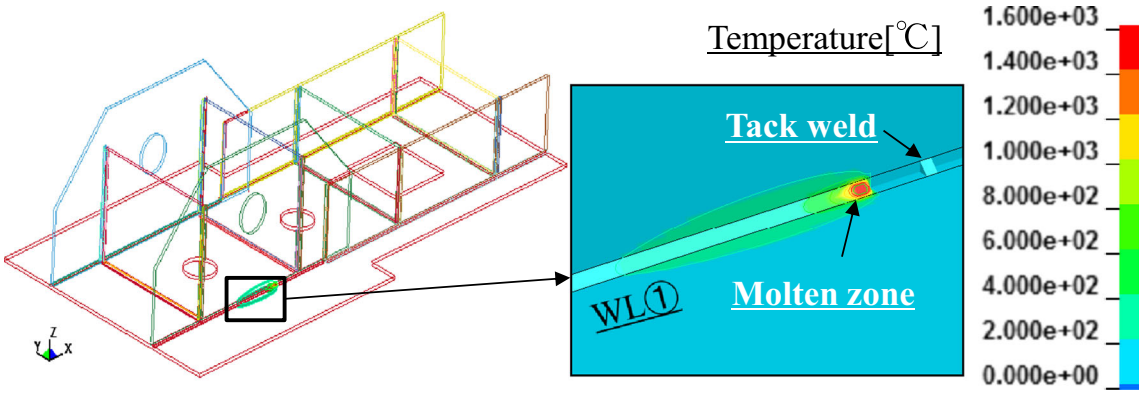

Fig. 22 A transient temperature field during welding longitudinal fillet WL①

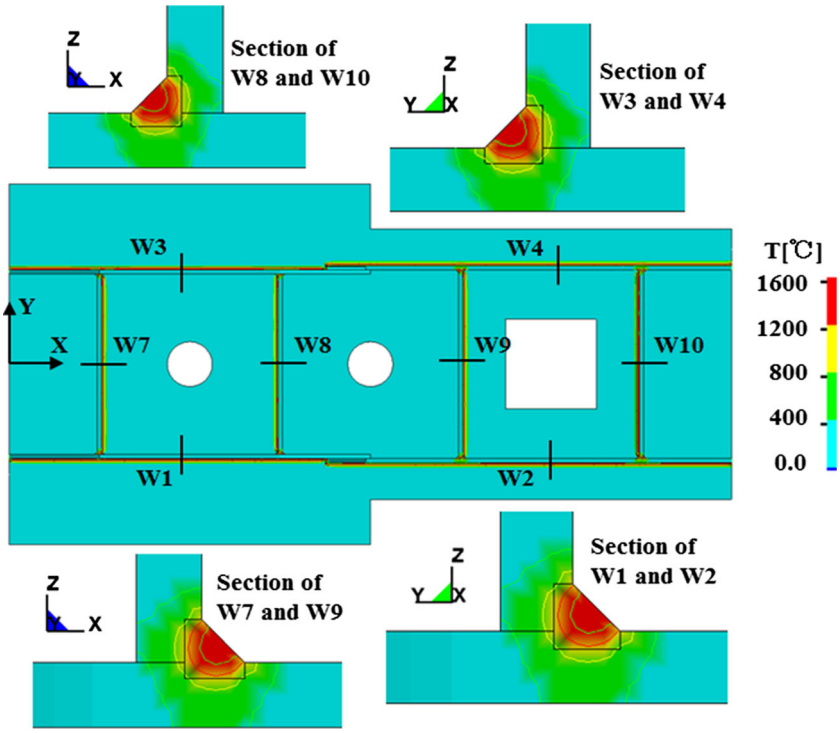

Fig. 23 Maximum temperature distribution in cross section of fillet welds (W1-W10)

to be the same as those at 1200 °C. The materials follow the isotropic linear hardening law and related plastic flow rule.

4.4 Temperature distributions and computation time for thermal elastic–plastic analysis

The welding thermal conduction analysis before thermal elastic–plastic analysis was performed using an in-house implicit FEM program JWRIAN [20] which was not programmed with GPU parallel computing and is not the topic in this work. Figure 22 shows a transient temperature field during welding of the weld line WL①. Figure 23 represents the distribution of the maximum reached temperature in the thermal cycles in the cross section of fillet welds (W1–W10). Figure 24 shows the maximum temperature distribution in the cross section of two lap welds (W5–W6) and fillet welds (W11–W26). Using the prepared transient temperature fields induced by all weld lines as an input data with 4196 thermal time steps, the thermal elastic–plastic analysis was performed using the ACEXP method with GPU parallel computing. Since the evaluation of this simulation was mainly focused on the residual welding deformation and stresses more than their transient values, the equilibrium computation was only conducted at the final step using ACEXP controlling parameters $t_{\text{scale}} = 1000, dT = 0.5$, $Nc = \infty$. When GPU board tesla-k20 was employed (2496 Cuda cores), the computing time only for thermal elastic–plastic analysis excluding thermal conduction analysis for all 26 weld lines was about 45 h with 2,167,517 explicit cycles and average computing time for each weld line was about 1.7 h. Currently, it is difficult to use one CPU or implicit FEM to

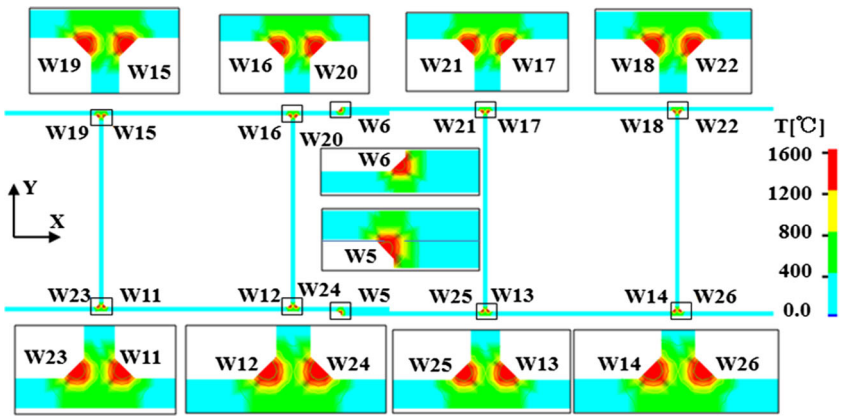

Fig. 24 Maximum temperature distribution in cross section of lap welds (W5-W6) and fillet welds (W11-W26)

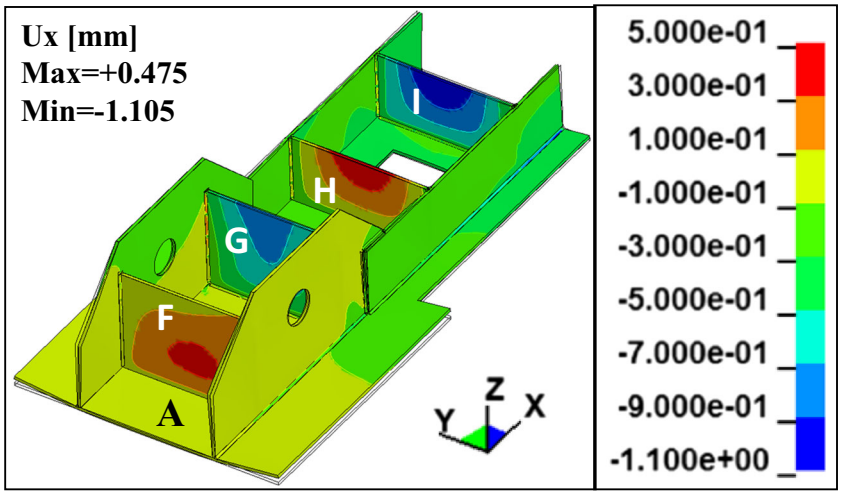

Fig. 25 Distribution of welding deformation component Ux by ACEXP method

compute the welding induced thermal stress and deformation in this large-scale model.

4.5 Welding deformation

Figure 25 shows the distribution of the x-displacement Ux of the welded structure by the ACEXP method with GPU parallel computing. The maximum displacement Ux towards to the +X direction and the −X direction is about 0.48 and −1.1 mm, respectively. The maximum plus displacement Ux occurred at the edge of transverse stiffener plate-H. The maximum minus displacement Ux existed at the edge of transverse stiffener plate-I. The large displacement Ux in transverse stiffener plates F~I was mainly induced by the single-side fillet weld lines ⑦~⑩.

From the distribution of the y-displacement Uy shown in Fig. 26, it can be known that the maximum displacement Uy is 1.9 mm which existed at the edges of longitudinal stiffener plates B, C, D, and E. The maximum displacement at the edges is mainly due to the longitudinal fillet weld lines ①~④ and their induced angular distortion.

Figure 27 represents the distribution of the displacement-Uz computed by the ACEXP method. It can be observed that there were large deflections on the bottom plate. The maximum deflection is about 5.4 mm which occurred at two edges of the bottom plate.

Figures 28, 29, and 30 represent the displacement Ux, Uy, and Uz and their comparisons with experimental measurements at all 96 evaluating points shown in Fig. 20. The computed displacements at evaluating points show the same deformation tendency as those by experimental measurement. The maximum displacements and their existing positions predicted by the ACEP method are close to those measured in experiments. Therefore, it can be understood that the proposed

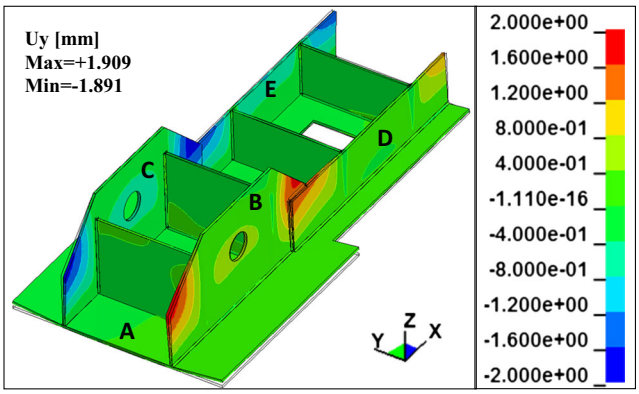

Fig. 26 Distribution of welding deformation component Uy by ACEXP method

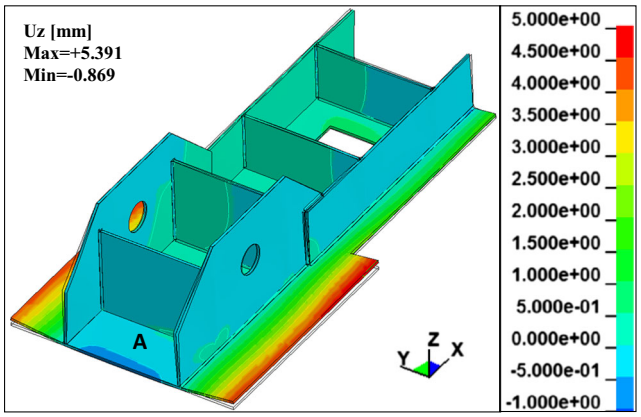

Fig. 27 Distribution of welding deformation component Uz by ACEXP method

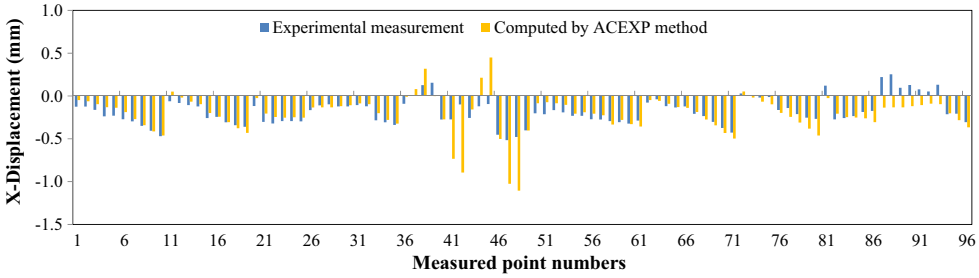

Fig. 28 Comparison of welding deformation (Ux) between computation and measurement.

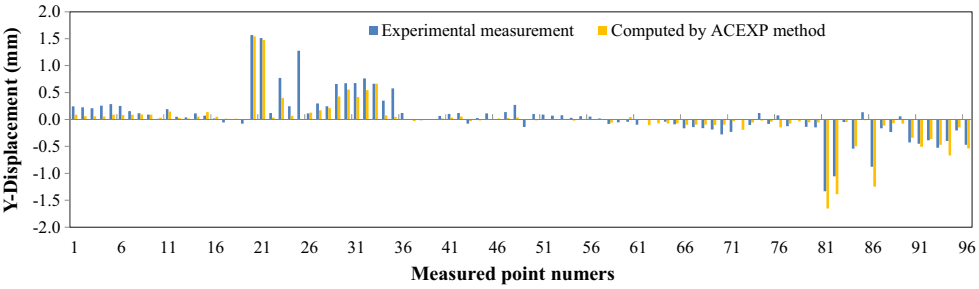

Fig. 29 Comparison of welding deformation (Uy) between computation and measurement

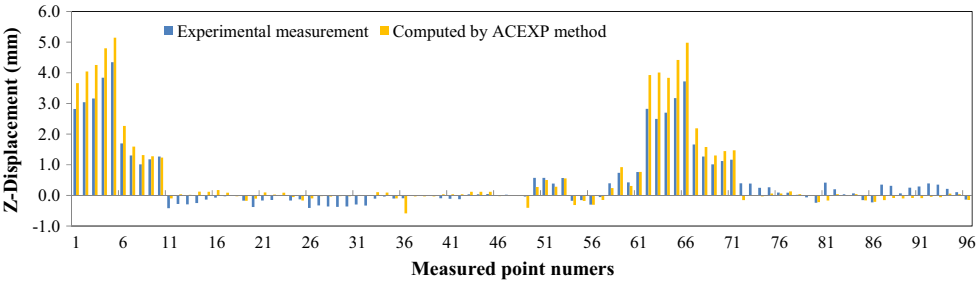

Fig. 30 Comparison of welding deformation (Uz) between computation and measurement

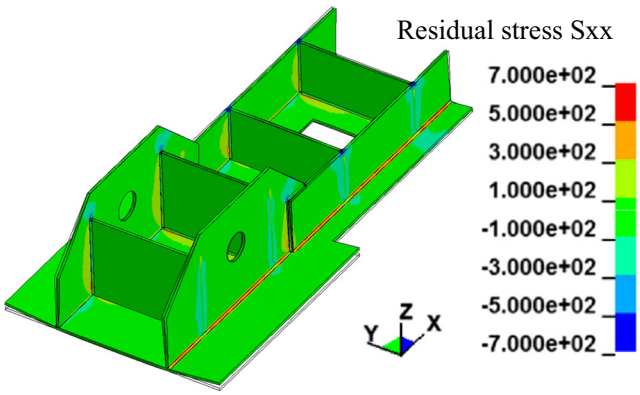

Fig. 31 Distribution of welding residual stress Sxx

ACEXP method is reliable to predict the welding deformation in welded structures.

4.6 Welding residual stresses

Figures 31, 32, and 33 show the distributions of residual stress components Sxx, Syy, and Szz, respectively. Tensile residual stresses existing around the welded zones reached the materials yield stress. Since the measurement of welding residual stresses in welded structures in structure models is difficult, the ACEXP method with GPU parallel computing can be a power tool to predict information of residual stresses for the strength evaluation of welded structures.

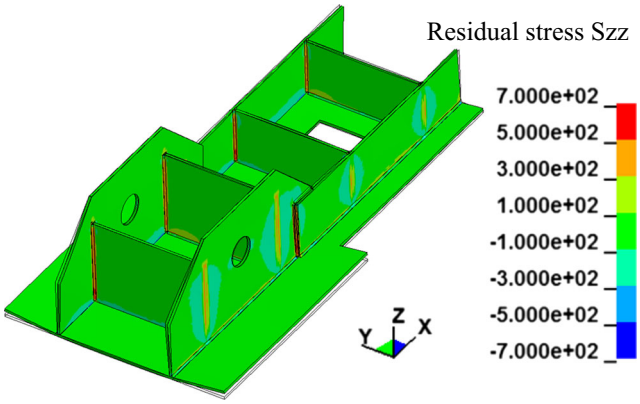

Fig. 32 Distribution of welding residual stress Syy

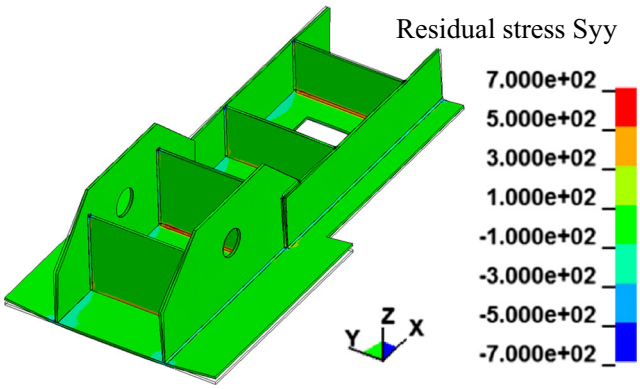

Fig. 33 Distribution of welding residual stress Szz

5 Summaries

(1) An accelerated explicit method and its GPU parallel computing FEM program for the prediction of welding induced thermal stress and deformation were developed using a two-stage computation scheme, i.e., a dynamic thermal loading computation stage and an equilibrium computation stage.

(2) A transient radial eigenvalue corresponding to the transient welding deformation was automatically computed using the integrated velocity of the FE model and a damping parameter was determined.

(3) The accelerated ratio using GPU parallel computing for the proposed explicit method is 25 times comparing with the computation time using one CPU core. The GPU computing for the proposed accelerated explicit method has the ability to simulate large scale FE models with more than 20 million DOFs.

(4) The proposed accelerated explicit method was verified by an implicit FEM using a basic bead-on-plate model through comparing the transient thermal stresses, thermal deformation, and their residual values.

(5) The transient thermal elastic–plastic phenomena in a structure model with 1.4 million DOFs and 26 weld lines was efficiently simulated within 45 h using the proposed accelerated explicit method with GPU computing.

(6) The welding deformation in a structure model with 26 weld lines predicted by accelerated explicit method agreed well compared with those by experimental measurement.

Acknowledgments Author would like to express the sincerely acknowledgement to Prof. H. Murakawa, Osaka University, and Associate Prof. M. Shibahara, Osaka Prefecture University, for their valuable comments and supports in developing the accelerated explicit method and GPU parallel computing program.

References

1. Radaj D, Sonsino CM, Fricke W (2006) Fatigue assessment of welded joints by local approaches (2nd Edition), Woodhead Publishing, ISBN-13: 978–1855739482.
2. Lai W, Pan J, Feng Z, Santella M, Pan T (2013) Failure mode and fatigue behavior of ultrasonic spot welds with adhesive in lap-shear specimens of magnesium and steel sheets. SAE Int J Mater Manf 6(2):279–285
3. Dong P, Hong JK (2004) The master S-N curve approach to fatigue of piping and vessel welds. Weld World 48(1):28–36
4. Ueda Y, Yamakawa T (1971) Analysis of thermal elastic–plastic stress and strain during welding by finite element method. Transactions of the Japan Welding Society 2(2):186–196
5. Ueda Y, Murakawa H, Nakacho K, Ma N (1995) Establishment of computational welding mechanics. Trans JWRI 24(2):73–86
6. Ueda Y, Murakawa H, Ma N (2012) Welding deformation and residual stress prevention. Butterworth-Heinemann, New York, USA
7. Hibbit HD, Marcal PV (1973) Numerical thermo-mechanical model for the welding and subsequent loading of a fabricated structure. Comput Struct 3:1145–1174
8. Goldak J, Chakravarti A, Bibby M (1984) A new finite element method for welding heat source. J Metallurgical and materials Transactions B 15:299–305
9. Jonsson M, Karlsson L, Lindgren LE (1985) Simulation of tack welding procedures in butt joint welding of plates. Weld J 64(10): 296–301
10. Brown S, Song H (1992) Finite element simulation of welding of large structures. J Eng Ind Trans ASME 114(11):441–451
11. Lindgren LE, Haggblad HA, MacDill JMJ, Oddy AS (1997) Automatic remeshing for three-dimensional finite element simulation of welding. Comp Meth Appl Mech Engineering 147:401–409
12. Nishikawa H, Oda I, Shibahara M, Serizawa H, Murakawa H (2004) Three-dimensional thermal-elastic–plastic FEM analysis for predicting residual stress and deformation under multi-pass welding, Proc. ISOPE04, Toulon, France.
13. Lindgren LE (2006) Numerical modelling of welding. Comput Methods Appl Mech Engrg 195(48):6710–6736
14. Murakawa H, Deng D, Ma N, Wang JC (2012) Applications of inherent strain and interface element to simulation of welding deformation in thin plate structures. Comp Mater Sci 51(1):43–52
15. Deng D, Murakawa H, Liang W (2007) Numerical simulation of welding distortion in large structures. Comput Methods Appl Mech Engineer 196(46):4613–4627
16. Wang JC, Ma N, Murakawa H (2015) An efficient FE computation for predicting welding induced buckling in production of ship panel structure. Mar Struct 41:20–52

17. Ma N, Wang JC (2015) Out-of-plane welding distortion prediction and mitigation in stiffened welded structures. Int J Adv Manuf Technol 80(5–8):1–19
18. Vega A, Escobar E, Fong A, Ma N, Murakawa H (2013) Analysis and prediction of parallel effect on inherent deformation during the line heating process. Comp Model Eng Sci 90(3):197–210
19. Goldak J, Asadi M (2011) Computational weld mechanics and optimization of welding procedures, welds and welded structures, Trans. JWRI, Special Issue on Welding Science and Engineering (WSE2011).
20. Murakawa H, Ma N, Huang H (2015) Iterative substructure method employing concept of inherent strain for large scale welding problem, Welding in the World, 59(1), DOI: 10.1007/s40194-014-0178-z
21. Huang H, Ma N, Hashimoto T, Murakawa H (2015) Welding deformation and residual stresses in arc welded lap joints by modified iterative analysis. Science and Technology of Welding and Joining 20(7):571–577
22. Ma N, Li LQ, Huang H, Chang S, Murakawa H (2015a) Residual stresses in laser-arc hybrid welded butt-joint with different energy ratios. J Mater Process Technol 220:36–45
23. Ma N, Huang H, Murakawa H (2015b) Effect of jig constraint position and pitch on welding deformation. J Mater Process Technol 221:154–162
24. Ma N, Cai ZP, Huang H, Deng D, Murakawa H, Pan JL (2015c) Investigation of welding residual stress in flash-butt joint of U71Mn rail steel by numerical simulation and experiment. Materials and Design 88:1296–1309
25. Hallquist JO (1977) A numerical procedure for three-dimensional impact problems, American Society of Civil Engineering, Preprint 2956.
26. Mahin KW, Winters W, Holden TM, Hosbons RR and Macewen SR (1988) Evaluation of residual stress distribution in a traveling GTA weld using finite element and experimental techniques, Modeling of Casting and Welding. Processes IV, Sheraton Palm Coast, Florida, USA
27. Ma N, Umezu Y, Murakawa H (1998) Analysis of thermal distortion and residual stresses in welding using LS-DYNA, Proc. 5th Int.LS-DYNA user's conference.
28. Ma N, Umezu Y (2008) Application of explicit FEM to welding deformation. Light Metal Welding Structures 46(4): 142–149
29. Shibahara M, Ikushima K, Ito S, Masaoka K (2011) Computational method for transient welding deformation and stress for large scale structure based on dynamic explicit FEM. Journal of Japan Welding Society 29(1):1–9
30. Ikushima K, Shibahara M (2014) Prediction of residual stresses in multi-pass welded joint using idealized explicit FEM accelerated by GPU. Computational Material Science 93(7):62–67
31. Courant R, Friedrichs K, Lewy H (1928) Über die partiellen Differenzengleichungen der mathematischen Physik. Mathematische Annalen 100(1):32–74
32. Paradrakakis M (1981) A method for the automated evaluation of the dynamic relaxation parameters. Comput Methods Appl Mech Engineer 25:35–48